

University of South Carolina Scholar Commons

Faculty Publications

Chemical Engineering, Department of

2007

Simulation of Polarization Curves for Oxygen Reduction Reaction in 0.5 M H₂SO₄ at a Rotating Ring Disk Electrode

Qingbo Dong

Shriram Santhanagopalan

Ralph E. White

University of South Carolina - Columbia, white@cec.sc.edu

Follow this and additional works at: https://scholarcommons.sc.edu/eche_facpub

 Part of the [Other Chemical Engineering Commons](#)

Publication Info

Published in *Journal of the Electrochemical Society*, Volume 154, Issue 8, 2007, pages A816-A825.

© The Electrochemical Society, Inc. 2007. All rights reserved. Except as provided under U.S. copyright law, this work may not be reproduced, resold, distributed, or modified without the express permission of The Electrochemical Society (ECS). The archival version of this work was published in

Dong, Q., Santhanagopalan, S., & White, R.E. (2007). Simulation of Polarization Curves for Oxygen Reduction Reaction in 0.5 M H₂SO₄ at a Rotating Ring Disk Electrode. *Journal of the Electrochemical Society*. 154(8), A816-A825.

Publisher's Version: <http://dx.doi.org/10.1149/1.2741056>

This Article is brought to you by the Chemical Engineering, Department of at Scholar Commons. It has been accepted for inclusion in Faculty Publications by an authorized administrator of Scholar Commons. For more information, please contact dillarda@mailbox.sc.edu.



Simulation of Polarization Curves for Oxygen Reduction Reaction in 0.5 M H₂SO₄ at a Rotating Ring Disk Electrode

Qingbo Dong,* Shriram Santhanagopalan, and Ralph E. White**^z

Department of Chemical Engineering, University of South Carolina, Columbia, South Carolina 29208, USA

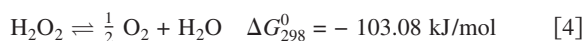
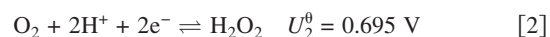
A cylindrical two-dimensional model based on the Nernst–Planck equations, the Navier–Stokes equation, and the continuity equation is used to simulate the oxygen reduction reaction in 0.5 M H₂SO₄ at a rotating ring disk electrode. Concentration distributions and a potential profile are obtained as a function of the axial and radial distances from the center of the electrode surface. Polarization curves are simulated to interpret experimental results by studying various reaction mechanisms, i.e., the four-electron-transfer reduction of oxygen, the two-electron-transfer reduction of oxygen, a combination of the above two reactions, mechanisms with reduction of peroxide to water, and/or the heterogeneous chemical decomposition of peroxide. Special attention is devoted to the effect of peroxide.

© 2007 The Electrochemical Society. [DOI: 10.1149/1.2741056] All rights reserved.

Manuscript submitted October 4, 2006; revised manuscript received March 26, 2007. Available electronically June 26, 2007.

Peroxide generated in the cathode of a proton exchange membrane fuel cell (PEMFC) can cause the failure of the membrane.^{1–3} Peroxide can be generated in the oxygen reduction reaction (ORR), which occurs in the cathode of a PEMFC. Because it is difficult to observe the presence of peroxide in the cathode of the fuel cell directly, the rotating disk ring electrode (RRDE) is used for studying the peroxide generation in the ORR in different acidic electrolytes such as sulfuric, perchloric, hydrochloric, and organic acid solutions.^{4–7} The merit of the RRDE technique in this application is that the amount of peroxide generated on the disk can be quantified by using the ring current.⁸

In an acidic environment, species are consumed or generated on the disk and the ring through four possible reactions which can be summarized by the following overall equations⁹



The U_j^0 is the standard electrode potential for the charge transfer reaction j in volts. Note that all of the potentials mentioned in this work are with respect to the standard hydrogen electrode. ΔG_{298}^0 is the standard Gibbs free energy change in a chemical process at 298 K in kJ/mol. According to the nature of the active catalyst and the operating conditions, these reactions take place at various rates. The direct 4e^- reduction of oxygen (Reaction 1) is the primary reaction in the ORR and it can be used to describe the system satisfactorily in cases such as when some low-index single-crystal surface platinum [for example, Pt(110)] electrodes are used.^{10,11} The 2e^- reduction (Reaction 2) may also occur solely in an acidic environment. When an S-modified platinum electrode is used, the oxygen reduction takes the 2e^- pathway and peroxide is the stable final product in the system, as shown in the work of Mo et al.¹² But in general, the ORR is a combination of Reactions 1 and 2, and the generated peroxide is consumed by electrochemical reduction, as shown by Reaction 3 and/or spontaneously decomposed to form oxygen as shown by Reaction 4. When two or more of the reactions occur simultaneously, various interesting phenomena show up in the polarization curves obtained experimentally with the RRDE.^{5,6,11,13–19} The polarization curves (either for the disk or the ring) often show a tail at the lower potential side (the absolute value of the disk current decreases and the value of the ring current in-

creases when the potential is below 0.2 V) and/or a hump in the potential at 0.4–0.6 V. (The absolute value of the disk current in this region decreases and then increases back to the original value.) Both the tail and the hump indicate the presence of peroxide, and this work attempts to explain these anomalies in terms of the reaction mechanism.

The hydrodynamic aspects of an RRDE were studied in depth by previous researchers, and analytical series solutions and one-dimensional numerical solutions were obtained.^{8,20–22} In this work, the hydrodynamics at an RRDE is solved with a cylindrical two-dimensional model based on the Navier–Stokes equation.²⁰ The Nernst–Planck equation is used to simulate the mass transport near the RRDE.^{21,23,24} All the basic transport terms, including diffusion and convection, and the migration term are retained in the Nernst–Planck equation to ensure accuracy. The kinetic equations used for the boundary conditions on the disk and the ring where the electrochemical reactions occur G_{298}^0 are based on the Butler–Volmer equation.^{25–27}

The simulation was carried out using the commercial software, COMSOL MultiPhysics (COMSOL MP). The model equations subject to the assigned boundary conditions are solved with the finite element method readily, and polarization curves are simulated for cases in which Reactions 1–4 occur to various extents. Concentration distributions of oxygen and peroxide and the potential profile near the surface of the electrode are presented.

Model Equations

A sketch of the cross section of the RRDE and the simulated domain adjacent to the electrode surface is shown in Fig. 1. The

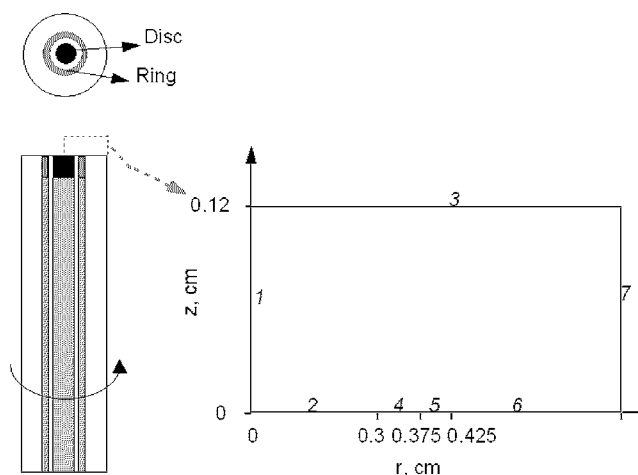


Figure 1. Schematic of an RRDE and the modeling domain.

* Electrochemical Society Student Member.

** Electrochemical Society Fellow.

^z E-mail: white@engr.sc.edu

variable z is used to represent the axial coordinate for which the origin is set at the surface of the electrode. The radial coordinate is represented by r and its origin is set at the axis of the electrode. According to the work of F. M. White, the velocity changes are negligible when the dimensionless distance ζ is greater than 10.²⁰ The dimensionless distance is defined by $\zeta = z\sqrt{\Omega/(\mu/\rho)}$, where Ω is the rotating speed of the electrode in rad/s, μ is the kinematic viscosity in mPa s, and ρ is the density of the electrolyte in g/cm³. Bard and Faulkner also suggested that a region of 0–7.2 ζ in the axial direction should be used for material balance.⁸ Therefore, $z = 0$ –0.12 cm ($z_{\infty,v} \approx 10\zeta$) is selected as the simulation domain. Numbers in italics in the schematic shown in Fig. 1 represent the boundaries as referenced in the following sections.

Momentum balance (swirl flow model).—The following assumptions are made in this model: the electrolyte is a Newtonian fluid with constant density and viscosity, the physical properties of the electrolyte (0.5 M H₂SO₄ saturated with pure oxygen at 1 atm and 298 K) can be approximated by those of water, and the system has axial symmetry and is at steady state. The generalized equations of motion and continuity in cylindrical coordinates are in the following form^{21,28}

$$\rho \frac{\partial \mathbf{u}}{\partial t} - \nabla \cdot \mu [\nabla \mathbf{u} + (\nabla \mathbf{u})^T] + \rho (\mathbf{u} \cdot \nabla) \mathbf{u} + \nabla P = 0 \quad [5]$$

$$\nabla \cdot \mathbf{u} = 0 \quad [6]$$

where P is the pressure in Pa, and \mathbf{u} is the velocity vector in cm/s. With the assumption of axial symmetry and steady-state flow, the derivatives with respect to time (t) and angular coordinate (θ) are all equal to zero. The density and viscosity are assumed to be constants. Equations 5 and 6 can then be simplified and written in the expanded form as follows^{8,20,21}

(Continuity equation)

$$\frac{1}{r} \frac{\partial}{\partial r} (ru_r) + \frac{\partial}{\partial z} (u_z) = 0 \quad [7]$$

(r component)

$$\rho \left(u_r \frac{\partial u_r}{\partial r} - \frac{u_\theta^2}{r} + u_z \frac{\partial u_r}{\partial z} \right) = - \frac{\partial P}{\partial r} + \mu \left[\frac{1}{r} \frac{\partial}{\partial r} \left(r \frac{\partial u_r}{\partial r} \right) - \frac{u_r}{r^2} + \frac{\partial^2 u_r}{\partial z^2} \right] \quad [8]$$

(θ component)

$$\rho \left(u_r \frac{\partial u_\theta}{\partial r} + \frac{u_r u_\theta}{r} + u_z \frac{\partial u_\theta}{\partial z} \right) = \mu \left[\frac{1}{r} \frac{\partial}{\partial r} \left(r \frac{\partial u_\theta}{\partial r} \right) - \frac{u_\theta}{r^2} + \frac{\partial^2 u_\theta}{\partial z^2} \right] \quad [9]$$

(z component)

$$\rho \left(u_r \frac{\partial u_z}{\partial r} + u_z \frac{\partial u_z}{\partial z} \right) = - \frac{\partial P}{\partial z} + \mu \left[\frac{1}{r} \frac{\partial}{\partial r} \left(r \frac{\partial u_z}{\partial r} \right) + \frac{\partial^2 u_z}{\partial z^2} \right] \quad [10]$$

where u_r is the radial component of the velocity in cm/s, u_θ is the angular component of the velocity in cm/s, and u_z is the axial component of the velocity in cm/s. The swirl flow problem is a two-dimensional problem with only two independent variables r and z , even though all three velocity components (in u_r , u_θ , and u_z) are modeled as shown in Eq. 7–10. These equations can be simplified further by introducing dimensionless variables.²⁰ However the original variables are retained in this work for two reasons: (i) retaining the original variables helps us to readily compare the results with experimentally measured variables, and (ii) making the variables dimensionless does not significantly improve the computational efficiency because COMSOL MP automatically scales the variables.

Mass balance (Nernst–Planck equations).—The following assumptions are made for the mass balance: the system is assumed to be at steady state; there are no homogeneous reactions; the axial symmetry condition is applicable; and the concentrations and liquid phase potential do not change at positions far away from the electrochemical reaction sites.

The general form of the Nernst–Planck equation used for the mass balance is as follows²¹

$$\nabla \cdot \left(-D_i \nabla c_i - z_i c_i F \frac{D_i}{RT} \nabla \Phi + c_i \mathbf{u} \right) = 0 \quad [11]$$

where c_i is the concentration of species i in mol/cm³ ($i = 1, 2, 3$, and 4 represent HSO₄[−], H₂O₂, H⁺, and O₂, respectively), D_i is the diffusion coefficient of the species “ i ” in cm²/s, z_i is the charge on species “ i ”, F is Faraday’s constant 96487 C/equiv, and Φ is the potential in the electrolyte in V. Under conditions of axial symmetry, Eq. 11 can be expanded as follows

$$u_r \frac{\partial c_i}{\partial r} + u_z \frac{\partial c_i}{\partial z} = D_i \left(\frac{\partial^2 c_i}{\partial z^2} + \frac{\partial^2 c_i}{\partial r^2} + \frac{1}{r} \frac{\partial c_i}{\partial r} \right) + z_i \frac{D_i}{RT} F \left[c_i \left(\frac{\partial^2 \Phi}{\partial z^2} + \frac{\partial^2 \Phi}{\partial r^2} + \frac{1}{r} \frac{\partial \Phi}{\partial r} \right) + \left(\frac{\partial c_i}{\partial r} + \frac{\partial c_i}{\partial z} \right) \left(\frac{\partial \Phi}{\partial r} + \frac{\partial \Phi}{\partial z} \right) \right] \quad [12]$$

Equation 12 can be written for each species corresponding to $i = 1, 2, 3$, and 4; but there are five variables including four concentrations (c_{1-4}) and the potential in the liquid phase (Φ) that need to be solved. In the calculation procedure, one of the concentrations (c_1 , the concentration of HSO₄[−]) is obtained from the electroneutrality condition

$$\sum_{i=1}^4 z_i c_i = 0 \quad [13]$$

and c_2 , c_3 , c_4 , and Φ are solved with the four equations represented by Eq. 12.

Boundary conditions for velocity and pressure.—Boundary 1 is at the axis of the cylindrical coordinate, and axial symmetry conditions are applicable

$$u_r = 0, u_\theta = 0, \quad \text{at } r = 0, \quad \forall z \quad [14]$$

Boundary 7 is far away from the axis of the cylindrical coordinate, and is treated as free surfaces (i.e., the viscous force is zero)

$$\mu (\nabla \mathbf{u} + (\nabla \mathbf{u})^T) \cdot \mathbf{n} = 0 \quad \text{at } r = 0.75 \text{ cm}, \quad \forall z \quad [15]$$

or, in the expanded form

$$\begin{aligned} -\mu \left(2 \frac{\partial u_r}{\partial r} \right) &= 0, & -\mu \left(r \frac{\partial}{\partial r} \left(\frac{u_\theta}{r} \right) \right) &= 0, \\ -\mu \left(\frac{\partial u_r}{\partial z} + \frac{\partial u_z}{\partial r} \right) &= 0, & \text{at } r = 0.75 \text{ cm}, \quad \forall z & \quad [16] \end{aligned}$$

Adjacent to the electrode, the no-slip conditions are assumed to apply, hence the r and z components of the velocity are set equal to zero, while the θ component of the velocity is set equal to the angular velocity of the electrode. So the velocities at boundaries 2, 4–6 are given by

$$u_r = 0, u_z = 0 \quad \text{and} \quad u_\theta = \Omega r \quad \text{at } z = 0, \quad \forall r \quad [17]$$

Only the first-order derivative of the pressure (P) exists in the governing equations (Eq. 3–6), which means that only one boundary condition in the z direction for pressure (P) is necessary.^{20,21} The pressure (P) is arbitrarily set to be zero at boundary 3. The derivative of velocity in z direction is equal to zero since the velocity has a constant value far from the surface of the electrode (boundary 3).^{20,21} Also u_r and u_θ can be set equal to zero at boundary 3 since there is no viscous effect far from the electrode surface (except an

axial inflow).²⁰ Accordingly, the following conditions for boundary 3 are given

$$u_r = 0, u_\theta = 0, P = 0, \frac{\partial u_z}{\partial z} = 0, \quad \text{at } z = 0.12 \text{ cm}, \quad \forall r \quad [18]$$

Boundary conditions for concentrations and potential.— Axial symmetry is used to set the boundary conditions at boundary 1, which is located at $r = 0$

$$\frac{\partial c_i}{\partial r} = 0, \quad \frac{\partial \Phi}{\partial r} = 0 \quad \text{at } r = 0, \quad \forall z \quad [19]$$

The concentrations at boundary 3, far away from the surface of the electrode, are the bulk concentrations ($c_{i, \text{bulk}}$, in mol/cm³), and the potential Φ is set equal to the potential of the reference electrode at the operating conditions (Φ_{RE} , in V)

$$c_i = c_{i, \text{bulk}}, \quad \Phi = \Phi_{\text{RE}} \quad \text{at } z = 0.12 \text{ cm}, \quad \forall r \quad [20]$$

At boundaries 2 and 5 which are adjacent to the disk and the ring, respectively, the reactions occur, and a jump material balance gives the following equations²⁵⁻²⁷

$$\left[D_i \frac{dc_i}{dz} + z_i c_i F \frac{D_i}{RT} \frac{d\Phi}{dz} \right] = \sum_{j=1}^3 \frac{s_{i,j} j_j}{n_j F} + s_{i,4} r_s \quad \text{for } i = 2, 3, 4$$

$$F \sum_{i=1}^4 z_i \left(-D_i \frac{dc_i}{dz} - z_i c_i F \frac{D_i}{RT} \frac{d\Phi}{dz} \right) = i_t \quad \text{at } r = 0 \sim 0.25$$

or $r = 0.325 \sim 0.375 \text{ cm}, z = 0$ [21]

where s_{ij} is the stoichiometric coefficient of species “ i ” in reaction “ j ”, j_j is the current density for reaction “ j ” in A/cm², i_t is the total current density in A/cm², n_j is the number of electrons transferred in reaction “ j ”, r_s is the chemical reaction (i.e., Reaction 4) rate at the electrode surface in mol/cm² s, R is the gas constant, 8.314 J/mol K, and T is the absolute temperature in K. In the first expression in Eq. 21, the left hand side is the mass flux of each species, and the right hand side is the generation or consumption of the respective species due to chemical and/or electrochemical reactions. In the second expression in Eq. 21, the left hand side is the net flux of charge in the electrolyte adjacent to the electrode surface, while the right hand side is the total current flow. At boundaries 4 and 6, the current will be zero, since there are no reactions occurring

$$0 = \left[D_i \frac{dc_i}{dz} + z_i c_i F \frac{D_i}{RT} \frac{d\Phi}{dz} \right] \quad \text{for } i = 2, 3, 4$$

$$0 = \sum_{i=1}^4 z_i \left(-D_i \frac{dc_i}{dz} - z_i c_i F \frac{D_i}{RT} \frac{d\Phi}{dz} \right) \quad \text{at } r = 0.25 \sim 0.325$$

or $r = 0.375 \sim 0.75 \text{ cm}, z = 0$ [22]

Boundary 7 is far away from the axis of the cylindrical coordinate, and the following conditions are applied

$$0 = \left[D_i \frac{dc_i}{dr} + z_i c_i F \frac{D_i}{RT} \frac{d\Phi}{dr} \right] \quad \text{for } i = 2, 3, 4$$

$$0 = \sum_{i=1}^4 z_i \left(-D_i \frac{dc_i}{dr} - z_i c_i F \frac{D_i}{RT} \frac{d\Phi}{dr} \right) \quad \text{at } r = 0.75, \quad \forall z \quad [23]$$

Note that z_i is equal to zero for neutral species O₂ and H₂O₂ ($i = 1$ and 2, respectively) in Eq. 21-23.

Kinetic equations.— The current densities in Eq. 21 can be obtained from the kinetic equations for the electrochemical reactions at the electrode surface based on the Butler–Volmer expression²⁵⁻²⁷

$$i_j = i_{0j, \text{ref}} \left\{ \prod_i \left(\frac{c_{i,0}}{c_{i, \text{ref}}} \right)^{p_{ij}} \exp \left(\frac{\alpha_{a,j} F}{RT} \eta_j \right) - \prod_i \left(\frac{c_{i,0}}{c_{i, \text{ref}}} \right)^{q_{ij}} \times \exp \left(- \frac{\alpha_{c,j} F}{RT} \eta_j \right) \right\} \quad [24]$$

where $i_{0j, \text{ref}}$ is the exchange current density due to reaction “ j ” at the reference concentrations in A/cm², $c_{i,0}$ is the concentration of species “ i ” adjacent to the surface of electrode in mol/cm³, $c_{i, \text{ref}}$ is the reference concentration of species “ i ” in mol/cm³, $\alpha_{a,j}$ is the anodic transfer coefficient for reaction “ j ”, $\alpha_{c,j}$ is the cathodic transfer coefficient for reaction “ j ”, p_{ij} is the anodic reaction order of species “ i ” in reaction “ j ”, q_{ij} is the cathodic reaction order of species “ i ” in reaction “ j ”, and η_j is the overpotential of reaction “ j ” in V, and it is measured with respect to a reference electrode of a given kind in a solution at the reference concentrations. The open circuit potential of reaction “ j ” at the reference concentrations relative to a standard reference electrode of a given kind is expressed as follows^{26,27}

$$U_{j, \text{ref}} = U_j^\theta - \frac{RT}{n_j F} \sum_i s_{i,j} \ln \left(\frac{c_{i, \text{ref}}}{\rho} \right) - U_{\text{RE}}^\theta + \frac{RT}{n_{\text{RE}} F} \sum_i s_{i, \text{RE}} \ln \left(\frac{c_{i, \text{RE}}}{\rho} \right) \quad [25]$$

where $s_{i, \text{RE}}$ is the stoichiometric coefficient of species “ i ” in the reaction occurring at the reference electrode, $U_{j, \text{ref}}$ is the open circuit potential of the reaction “ j ” at the reference concentrations relative to a standard reference electrode of a given kind in V, U_{RE}^θ is the potential of the standard reference electrode, $c_{i, \text{RE}}$ is the concentration of species “ i ” at the reference electrode in mol/cm³, n_{RE} is the number of electrons transferred in the reaction that occurs at the reference electrode. The overpotential for electrochemical reaction “ j ”, (η_j) in Eq. 24 is given by

$$\eta_j = \Phi_{\text{met}} - \Phi_{\text{RE}} - (\Phi_0 - \Phi_{\text{RE}}) - U_{j, \text{ref}} \quad [26]$$

where Φ_0 is the potential in the solution adjacent to the electrode surface in V, Φ_{met} is the potential of working electrode in V. The reaction orders $p_{i,j}$ and $q_{i,j}$ in Eq. 24 are related to $s_{i,j}$ by

$$\begin{cases} p_{i,j} = s_{i,j} & q_{i,j} = 0 & \text{if } s_{i,j} > 0 \\ p_{i,j} = 0 & q_{i,j} = -s_{i,j} & \text{if } s_{i,j} < 0 \end{cases} \quad [27]$$

The apparent transfer coefficients for reaction “ j ” sum up to the number of electrons transferred in that reaction, that is

$$\alpha_{a,j} + \alpha_{c,j} = n_j \quad [28]$$

The total current density is the sum of the partial current densities

$$i_t = \sum_{j=1}^3 i_j \quad [29]$$

The rate of the catalytic decomposition of peroxide at the electrode surface is expressed as

$$r_s = -k_h c_{\text{H}_2\text{O}_2,0}^p \quad [30]$$

where the reaction order (p) can be a fraction or a whole number, and it is assumed to be 1 in this work. The rate constant k_h is assumed to be independent of the applied potential (E_{appl} , or $\Phi_{\text{met}} - \Phi_{\text{RE}}$). Summaries of the governing equations and the boundary conditions (including the kinetic equations) are listed in Tables I and II, respectively.

Results and Discussion

The governing equations (Eq. 7-10, 12, and 13) subject to the given boundary conditions (Eq. 14-23) are solved numerically using COMSOL MP. The kinetic parameters, reaction properties, and physical properties of the species used in this simulation are shown in Table III. The constants, solution properties, and the operating conditions are listed in Table IV. The simulations were carried out for individual Reactions 1 and 2 as well as combinations of Reac-

Table I. Summary of the governing equations.

Governing equations for velocity and pressure	$\frac{1}{r} \frac{\partial}{\partial r}(ru_r) + \frac{\partial}{\partial z}(u_z) = 0$ $\rho \left(u_r \frac{\partial u_r}{\partial r} - \frac{u_\theta^2}{r} + u_z \frac{\partial u_r}{\partial z} \right) = -\frac{\partial p}{\partial r} + \mu \left(\frac{1}{r} \frac{\partial}{\partial r} \left(r \frac{\partial u_r}{\partial r} \right) - \frac{u_r}{r^2} + \frac{\partial^2 u_r}{\partial z^2} \right)$ $\rho \left(u_r \frac{\partial u_\theta}{\partial r} + \frac{u_r u_\theta}{r} + u_z \frac{\partial u_\theta}{\partial z} \right) = \mu \left(\frac{1}{r} \frac{\partial}{\partial r} \left(r \frac{\partial u_\theta}{\partial r} \right) - \frac{u_\theta}{r^2} + \frac{\partial^2 u_\theta}{\partial z^2} \right)$ $\rho \left(u_r \frac{\partial u_z}{\partial r} + u_z \frac{\partial u_z}{\partial z} \right) = -\frac{\partial p}{\partial z} + \mu \left(\frac{1}{r} \frac{\partial}{\partial r} \left(r \frac{\partial u_z}{\partial r} \right) + \frac{\partial^2 u_z}{\partial z^2} \right)$
Governing equations for concentration and potential	$u_r \frac{\partial c_i}{\partial r} + u_z \frac{\partial c_i}{\partial z} = D_R \left(\frac{\partial^2 c_i}{\partial z^2} + \frac{\partial^2 c_i}{\partial r^2} + \frac{1}{r} \frac{\partial c_i}{\partial r} \right) + z_i \frac{D_i}{RT} F \left[c_i \left(\frac{\partial^2 \Phi}{\partial z^2} + \frac{\partial^2 \Phi}{\partial r^2} + \frac{1}{r} \frac{\partial \Phi}{\partial r} \right) + \left(\frac{\partial c_i}{\partial r} + \frac{\partial c_i}{\partial z} \right) \left(\frac{\partial \Phi}{\partial r} + \frac{\partial \Phi}{\partial z} \right) \right]$ <p>where $i = 1, 2, 3, 4$ with respect to HSO_4^-, H_2O_2, H^+, and O_2</p> $\sum_i z_i c_i = 0$

tions 1-4 as listed in Table V. These reactions or reaction combinations are used to capture phenomena observed in polarization curves obtained experimentally in the literature.

Case (i): Four-electron transfer reduction (Reaction 1).—Reaction 1 is the basic reaction of the ORR at an RRDE in an acidic electrolyte, and it can be used to simulate the experimentally obtained polarization curves approximately. The solid lines marked with open circles in Fig. 2 are simulation results for Reaction 1 only with parameters $i_{0,1} = 1 \times 10^{-9} \text{ A/cm}^2$ and $\alpha_{c,1} = 1$. There is no current on the ring since there is no peroxide generated. The curve for disk current follows the trends for that of single reaction systems.²⁷ This means the polarization curve shifts towards more cathodic potentials if $i_{0,1}$ gets smaller as the overall reaction rate is slower. On the other hand, when $i_{0,1}$ is increased, it shifts towards more anodic potentials. The potential drop in the ohmic region will be drastic when the transfer coefficient ($\alpha_{c,1}$) is large, and the drop is mild when $\alpha_{c,1}$ is small.

Case (ii): Two-electron transfer reduction (Reaction 2).—In cases where peroxide is a stable product, Reaction 2 can be used to simulate the polarization curves. A set of simulated polarization curves for Reaction 2 are shown in Fig. 2 and are represented by lines marked with triangles. The current gathered on the ring is positive due to the anodic reaction and the current gathered on the disk is negative due to the cathodic reaction. Reaction 2 is reversible under the given operating conditions. The oxygen transferred to the disk surface is reduced to peroxide at a rate depending on the applied potential (E_{appl}) and the mass transfer limitations. When the peroxide is transferred to the ring on which a constant potential of 1.2 V is applied, it is oxidized back to oxygen. The collection efficiency N of an RRDE is defined by

$$N = \frac{I_R}{I_D} \quad [31]$$

where I_R is the limiting current collected on the ring in A, I_D is the limiting current collected on the disk in A, when a single reversible reaction is occurring on the disk and all the product collected on the ring can be converted back to the reactant. The value of N for the RRDE with dimensions shown in Fig. 1 obtained with the analytical calculation method developed by Albery et al. is 0.24.^{29,30} The value of N obtained in the simulation for Reaction 2 only in this work is 0.25. The experimental result published by Markovic et al. was 0.23.¹¹ These values for N are in good agreement. The limiting current predicted by Levich equation

$$I_L = 0.620nFAD\text{O}_2^{2/3}\omega^{1/2}\nu^{-1/6}c_{\text{O}_2\text{bulk}} \quad [32]$$

is $-5.32 \times 10^{-4} \text{ A}$. However, the limiting current obtained in this simulation work is $-5.15 \times 10^{-4} \text{ A}$. The discrepancy arises from the truncated series solutions for the velocities²² (of the order of z^3 for u_z and of z^2 for u_r) used in deriving the Levich equation. The velocity profile obtained in this work using the swirl flow model is consistent with the numerical solution of the one-dimensional model given by F. M. White.²⁰ We also verified that the simulations with truncated series solutions for the velocities and the Nernst–Planck equation for material balance will result in the same limiting current value as the Levich equation prediction (i.e., $I_L = -5.32 \times 10^{-4} \text{ A}$).

Case (iii): Competition between the four-electron transfer reduction and the two-electron transfer reduction (Reactions 1 and 2).—There are three possibilities when Reactions 1 and 2 compete with each other, as shown in Fig. 3a-c, corresponding to $\alpha_{c,2} > \alpha_{c,1}$, $\alpha_{c,2} = \alpha_{c,1}$ and $\alpha_{c,2} < \alpha_{c,1}$, respectively. The cathodic transfer coefficients (α_c) are in the exponential terms in the Butler–Volmer equation (Eq. 24), which means that they have a greater effect on the current than the exchange current densities ($i_{0,j}$) do when the overpotential (η_j) becomes sufficiently large.

When $\alpha_{c,2} > \alpha_{c,1}$, as in Fig. 3a, the absolute values of the disk currents in the mass transport limiting region decrease as the applied potential shifts towards 0 V. They decrease to different extents and start from different potentials, depending on the value of the exchange current density for Reaction 2 ($i_{0,2}$). These phenomena show up in the mass transport limiting region in which the oxygen flux to the electrode surface is constant and is at the maximum value. The reaction rates of the two reactions change while the total available reactant oxygen is constant when the applied potential (E_{appl}) decreases from about 0.7 V to 0 V. When the applied potential (E_{appl}) is high (about 0.7 V), Reaction 1 predominates and all the available reactant will be converted to water by a four-electron transfer process. When the applied potential (E_{appl}) is lower, Reaction 2 occurs at an observable rate and a part of the reactant (O_2) is converted to peroxide by two-electron transfer process. The total charge transferred in the process decreases and the absolute value of the disk current decreases, leading to a tail in the polarization curve for the disk. In the meantime more peroxide is generated on the disk and oxidized back on the ring, causing the ring current to increase. Ideally, if the applied potential (E_{appl}) is continuously lowered, Reaction 2 will dominate, eventually all of the oxygen will go to peroxide, and the polarization curve of the disk will reach a constant value again corresponding to the value of the limiting current of Reaction

Table II. Summary of the boundary conditions.

Boundary 1	$u_r = 0, u_\theta = 0$, at $r = 0$, all z
Boundary 7	$-\mu \left(2 \frac{\partial u_r}{\partial r} \right) = 0, -\mu \left(r \frac{\partial}{\partial r} \left(\frac{u_\theta}{r} \right) \right) = 0$, $-\mu \left(\frac{\partial u_r}{\partial z} + \frac{\partial u_z}{\partial r} \right) = 0$, at $r = 0.75$ cm, $\forall z$
Boundaries 2, 4-6	$u_r = 0, u_z = 0, u_\theta = \Omega r$, at $z = 0$, all r
Boundary 3	$u_r = 0, u_\theta = 0, P = 0$ at $z = 0.12$ cm for all r
Boundary 1	$\frac{\partial c_i}{\partial r} = 0, \frac{\partial \Phi}{\partial r} = 0$ at $r = 0$, all z
Boundary 3	$c_i = c_{i,\text{bulk}}, \Phi = \Phi_{\text{re}}$ at $z = 0.12$ cm, all r
Boundaries 2 and 5	$\sum_{j=1}^3 \frac{s_{i,j} j}{n_j F} + s_{i,4} r_s = \left[D_i \frac{dc_i}{dz} + z_i c_i F \frac{D_i}{RT} \frac{d\Phi}{dz} \right]$ for $i = 2, 3, 4$ $i_i = F \sum_{i=1}^4 z_i \left(-D_i \frac{dc_i}{dz} - z_i c_i F \frac{D_i}{RT} \frac{d\Phi}{dz} \right)$ at $r = 0 \sim 0.25$ or $r = 0.325 \sim 0.375$ cm, $z = 0$
Boundaries 4 and 6	$0 = \left[D_i \frac{dc_i}{dz} + z_i c_i F \frac{D_i}{RT} \frac{d\Phi}{dz} \right]$ for $i = 2, 3, 4$ $0 = \sum_{i=1}^4 z_i \left(D_i \frac{dc_i}{dz} + z_i c_i F \frac{D_i}{RT} \frac{d\Phi}{dz} \right)$ at $r = 0.25 \sim 0.325$ or $r = 0.375 \sim 0.75$ cm, $z = 0$
Boundary 7	$0 = \left[D_i \frac{dc_i}{dr} + z_i c_i F \frac{D_i}{RT} \frac{d\Phi}{dr} \right]$ for $i = 2, 3, 4$ $0 = \sum_{i=1}^4 z_i \left(-D_i \frac{dc_i}{dr} - z_i c_i F \frac{D_i}{RT} \frac{d\Phi}{dr} \right)$ at $r = 0.75$, $\forall z$
Butler-Volmer equation	$i_j = i_{o,j,\text{ref}} \left\{ \prod_i \left(\frac{c_{i,0}}{c_{i,\text{ref}}} \right)^{p_{i,j}} \exp \left(\frac{\alpha_{a,j} F}{RT} \eta_j \right) - \prod_i \left(\frac{c_{i,0}}{c_{i,\text{ref}}} \right)^{q_{i,j}} \exp \left(-\frac{\alpha_{c,j} F}{RT} \eta_j \right) \right\}$
Overpotential	$\eta_j = \Phi_{\text{met}} - \Phi_{\text{RE}} - (\Phi_0 - \Phi_{\text{RE}}) - U_{j,\text{ref}}$
Reference electrode potential	$U_{j,\text{ref}} = U_j^0 - \frac{RT}{n_j F} \sum_i s_{i,j} \ln \left(\frac{c_{i,\text{ref}}}{\rho} \right) - U_{\text{RE}}^0 + \frac{RT}{n_{\text{RE}} F} \sum_i s_{i,\text{RE}} \ln \left(\frac{c_{i,\text{RE}}}{\rho} \right)$
Reaction orders	$\begin{cases} p_{i,j} = s_{i,j} & q_{i,j} = 0 & \text{if } s_{i,j} > 0 \\ p_{i,j} = 0 & q_{i,j} = -s_{i,j} & \text{if } s_{i,j} < 0 \end{cases}$
Chemical reaction (Reaction 4)	$r_s = -k_h c_{\text{H}_2\text{O}_2,0}^p$

2 only. The ORR cannot be operated practically at potentials below 0 V, where other reactions such as hydrogen evolution prevail. Hence, our simulations were stopped at 0 V and so the tails do not reach constant values in Fig. 3a.

When $\alpha_{c,2} = \alpha_{c,1}$, as the applied potential (E_{appl}) drops, the absolute value of the disk current decreases and the value of the current at the ring increases when the open circuit potential (OCP) of Reaction 2 is reached, and then they reach a constant value as shown in Fig. 3b. However this constant value does not correspond to the limiting current for Reaction 2; it holds a value between the limiting currents of Reactions 1 and 2 as determined by the ratio of the exchange current densities ($i_{0,1}$ and $i_{0,2}$). The current does not change with the applied potential (E_{appl}) in the mass transport lim-

iting region, which implies that the rates of Reactions 1 and 2 do not change and a constant fraction of the reactant oxygen goes to peroxide.

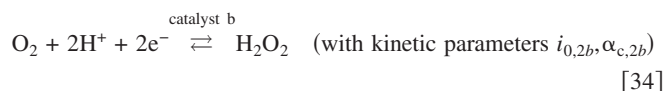
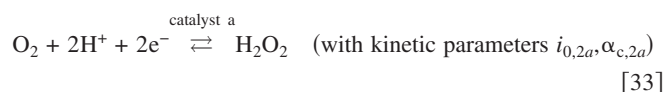
The case of $\alpha_{c,2} < \alpha_{c,1}$ is shown in Fig. 3c. When $i_{0,2}$ has a value big enough (about 1×10^{-6} A/cm² in this case), the current for the ring will rise and then drop down as the potential decreases, forming a hump on the curve. A similar phenomenon occurs on the disk current, although the size of the hump is smaller visually due to the scale of the ordinate in the figure. As shown in Fig. 3c, larger values for exchange current density for Reaction 2 ($i_{0,2}$) lead to a larger hump. The hump in the polarization curves due to Reaction 2 is visible when its rate is comparable with the rate of Reaction 1 in the potential region around 0.6 V to 0.4 V. It is worth noting that

Table III. Kinetic parameters, reaction properties, and physical properties of the species used for simulating the ORR in 0.5 M H₂SO₄.

Kinetic parameters	Reaction 1	Reaction 2	Reaction 3	Reaction 4
α_{ej}	1.0	0.8–1.2	0.25–0.45	
$i_{o,ref}$ (A/cm ²)	10 ⁻⁹	10 ⁻⁴ ~ 10 ⁻⁹	10 ⁻¹⁵ ~ 10 ⁻¹⁹	
U_j^0 (V) ⁹	1.229	0.695	1.736	
n_j	4	2	2	
k_h mol/s (mol/cm ³)				10 ⁻¹ ~ 10 ⁰
p				1
Reaction properties	HSO ₄ ⁻	H ₂ O ₂	H ⁺	O ₂
$s_{i,1}$	0	0	-4	-1
$s_{i,2}$	0	+1	-2	-1
$s_{i,3}$	0	-1	-2	0
$s_{i,4}$	0	1	0	-0.5
z	-1	0	+1	0
Solution properties	HSO ₄ ⁻	H ₂ O ₂	H ⁺	O ₂
$c_{i,ref}$ (mol/cm ³)	0.00051	1.377 × 10 ⁻¹⁴	0.0005	0.13 × 10 ⁻⁶
D_i (cm ² /s) ^{21,33}	1.33 × 10 ⁻⁵	1.16 × 10 ⁻⁵	9.312 × 10 ⁻⁵	1.79 × 10 ⁻⁵

this phenomenon can only occur in this potential region (around 0.6 V to 0.4 V), which is just below the OCP of Reaction 2. The exponential term in the cathodic part of the Butler–Volmer equation (Eq. 20) for Reaction 1 increases faster than that of Reaction 2, and the rate of Reaction 2 will not be comparable with that of Reaction 1 when the applied potential (E_{appl}) shifts further to cathodic values.

In polarization curves obtained experimentally, humps and tails show up together frequently. It is possible that more than one material in the catalyst prompts the ORR.^{5,31,32} For example, platinum is a known effective catalyst for ORR and it is often made in nanometer size particles and supported on carbon particles, such as the commercialized Pt/Vulcan catalyst powder by E-TEK. Carbon is suspected to have catalytic activity^{5,13} to prompt the two-electron transfer reaction (Reaction 2), and can cause the hump starting at about 0.6 V. To simulate the existence of additional catalytic active material for Reaction 2, it is treated as two separate reactions



The currents for Reactions 33 and 34 are written individually using Eq. 24. The combination of Reactions 1, 33, and 34 is simulated and

Table IV. Constants, solution properties and operation conditions used for the simulations.

F	96487 C/mol
R	8.314 J/K-mol
T	298.15 K
U_{RE}^0	0 V
ρ_0	0.001 kg/cm ³
ν	0.012 cm ² /s
Ω	900 rpm
Applied potential on ring	1.2 V

Table V. List of reactions and reaction combinations simulated.

Case number	Reactions involved
i	1
ii	2
iii	1, 2
iv	1, 2, 3
v	1, 2, 4
vi	1, 2, 4, and 1, 2, 3, 4

a set of the results are shown as solid lines in Fig. 4. The dashed and dotted lines in Fig. 4 are simulation results for the combination of Reactions 1 and 33 and the combination of Reactions 1 and 34, respectively. The values on the solid line for the ring are just a linear summation of values on the dashed line and the dotted line for the ring.

Case (iv): Competition involving peroxide reduction (Reactions 1-3).—Figure 5 shows the effect of Reaction 3 on the competition between Reactions 1 and 2. The cathodic transfer coefficients for Reactions 1 and 2 are equal in this simulation so the polarization curves should be the same as the curves marked with triangles in Fig. 3b if there were only Reactions 1 and 2. When Reaction 3 is involved, the limiting current shows a hump as shown in Fig. 5. This is because Reaction 3 converts the peroxide generated by Reaction 2 to water by a two-electron transfer process. Reaction 2 followed by Reaction 3 is equivalent to Reaction 1. The apparent result is that Reaction 1 is enhanced and Reaction 2 is weakened, and the polarization curves are similar to those shown in the case of $\alpha_{c,2} < \alpha_{c,1}$ (see Fig. 3c). Reaction 3 can reduce the size or change the positions of the humps and the tails as shown in Fig. 3a and c for similar reasons.

The polarization curves marked with squares in Fig. 5 are used for studying the contributions of Reactions 1-3 to the total current,

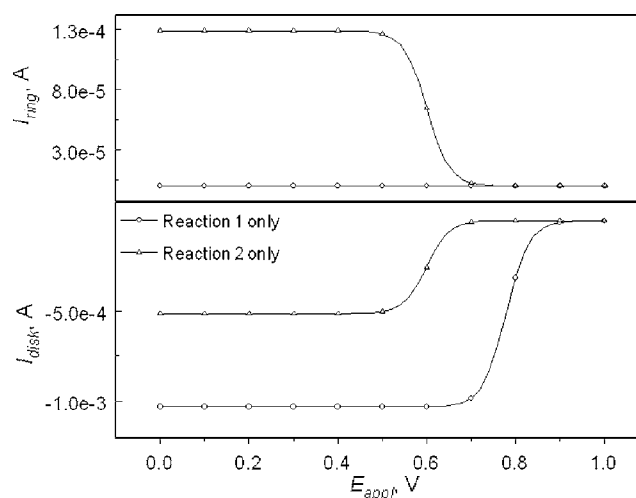


Figure 2. Polarization curves for single reactions: Comparison of four-electron transfer reaction and two-electron transfer reaction. Parameters used: $i_{0,1} = 1 \times 10^{-9}$ A/cm², $\alpha_{c,1} = 1.0$ for Reaction 1 only, $i_{0,2} = 1 \times 10^{-8}$ A/cm², $\alpha_{c,2} = 1.0$ for Reaction 2 only.

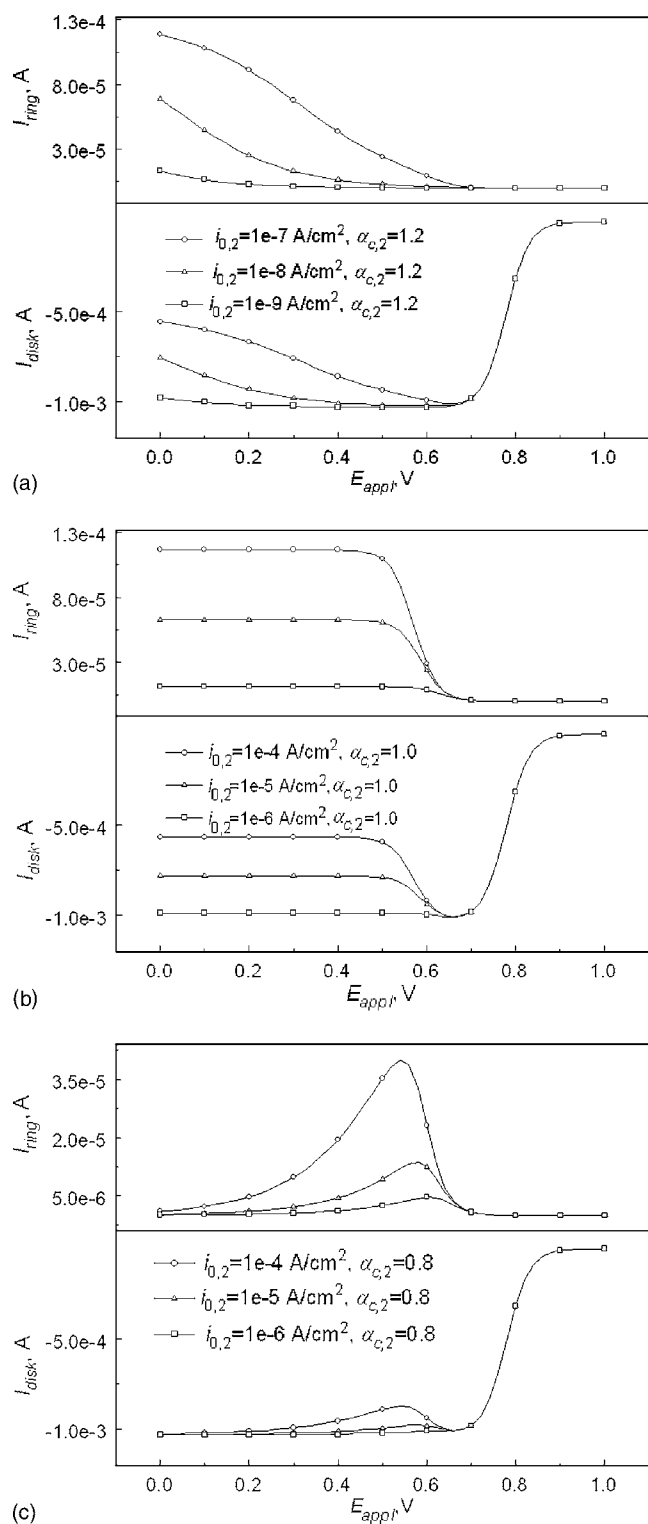


Figure 3. Polarization curves for competing Reactions 1 and 2. Parameters used: $i_{0,1} = 1 \times 10^{-9}$ A/cm², $\alpha_{c,1} = 1.0$, case a: $\alpha_{c,2} = 1.2$ for $\alpha_{c,2} > \alpha_{c,1}$; case b: $\alpha_{c,2} = 1.0$ for $\alpha_{c,2} = \alpha_{c,1}$; case c: $\alpha_{c,2} = 0.8$ for $\alpha_{c,2} < \alpha_{c,1}$.

and the results are shown in Fig. 6. The total disk current is just the summation of the currents for the three individual Reactions 1-3. Under the given simulation conditions, only Reaction 2 occurs on the ring and the current from this reaction is the only component of the ring current.

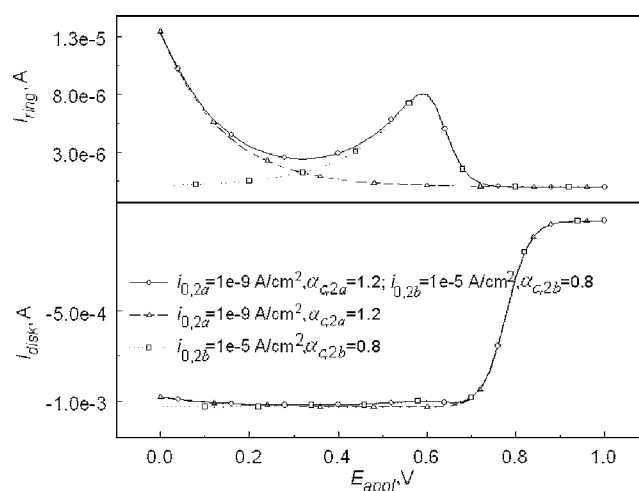


Figure 4. Polarization curves for competing Reactions 1, 33, and 34. Parameters used: $i_{0,1} = 1 \times 10^{-9}$ A/cm², $\alpha_{c,1} = 1.0$.

Case (v): Competition involving chemical decomposition of peroxide (Reactions 1, 2, and 4, or 1-4).—Figure 7 shows the effect of Reaction 4, which is a heterogeneous chemical reaction in which peroxide is oxidized back to oxygen on the surface of the disk without involving charge transfer. The result is to shift the limiting current towards the one related to Reaction 1 since less peroxide is captured on the ring. Since this reaction is not related to potential, it will not change the shape of the polarization curve substantially, except to lower the flat lines in the limiting current region, reduce the size of humps, or move the tails to more cathodic potentials. The extent of these changes depends on the rate of Reaction 4.

Reactions 1-4 may occur simultaneously in the ORR system.^{9,24} This comprehensive situation is simulated in Fig. 8. All four reactions are effective and the rates of Reactions 1-3 are fixed, while the rate of Reaction 4 is changed by varying the rate constant k_h . The effect of Reaction 4 is as discussed in the above paragraph. The hump size reduces when the rate of Reaction 4 increases since peroxide is consumed. The essential shape of the polarization curves will depend on the kinetic parameters for Reactions 1-3.

The mechanism involving Reaction 3 and/or Reaction 4 can also be used to explain the hump and the tail phenomena. It is not evident from the experimental polarization curves whether Reaction 3 and/or Reaction 4 are involved when a hump and/or a tail shows.

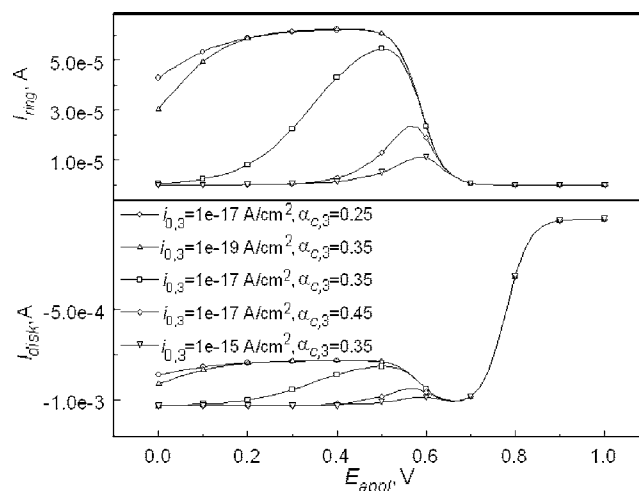


Figure 5. Polarization curves for competing Reactions 1-3. Parameters used: $i_{0,1} = 1 \times 10^{-9}$ A/cm², $\alpha_{c,1} = 1.0$, $i_{0,2} = 1 \times 10^{-5}$ A/cm², $\alpha_{c,2} = 1.0$.

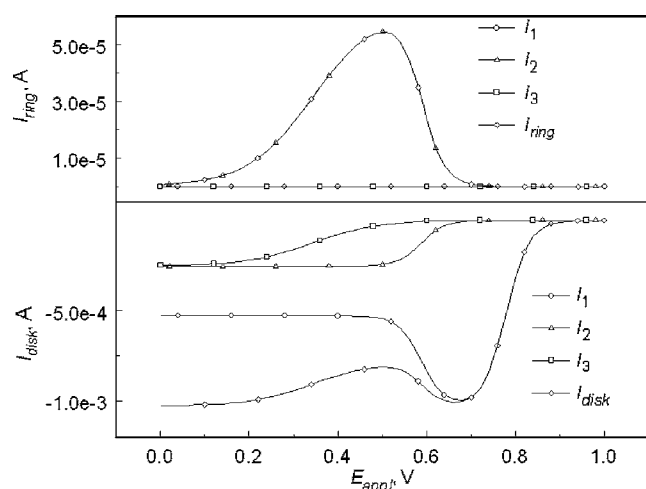


Figure 6. The contributions of Reactions 1-3 to the total current. Parameters used: $i_{0,1} = 1 \times 10^{-9}$ A/cm², $\alpha_{c,1} = 1.0$, $i_{0,2} = 1 \times 10^{-5}$ A/cm², $\alpha_{c,2} = 1.0$, $i_{0,3} = 1 \times 10^{-17}$ A/cm², $\alpha_{c,3} = 0.35$.

Although there are experimental results that show the coexistence of more than one reaction in the literature,^{9,21} no conclusive evidence has been reported that favors one mechanism over the others. This makes the ORR complicated.

Oxygen and peroxide concentration distributions and potential distribution.—Investigating the concentration and potential distributions can help us to gain some insight into the phenomena that occur during oxygen reduction in an RRDE system. Examples of concentration distributions of oxygen and peroxide are shown in Fig. 9. The parameters used are the same as those in Fig. 6, except that the applied potential (E_{appl}) is fixed at 0.5 V. Adjacent to the surface of the disk ($r = 0 - 0.3$ cm, $z = 0$), the concentration of oxygen (c_{O_2}) is near zero due to its consumption by the ORR. Away from the disk ($r > 0.3$ cm, $z = 0$), c_{O_2} rises up since oxygen is not consumed anymore and it is continuously transported toward the surface of the electrode from the bulk solution. Especially, adjacent to the surface of the ring ($r = 0.375 - 0.425$ cm), there is a jump in the concentration of oxygen because of the generation of oxygen at the ring. Far away from the disk along the r direction, c_{O_2} reaches the same value as in the bulk. The distribution of peroxide concentration

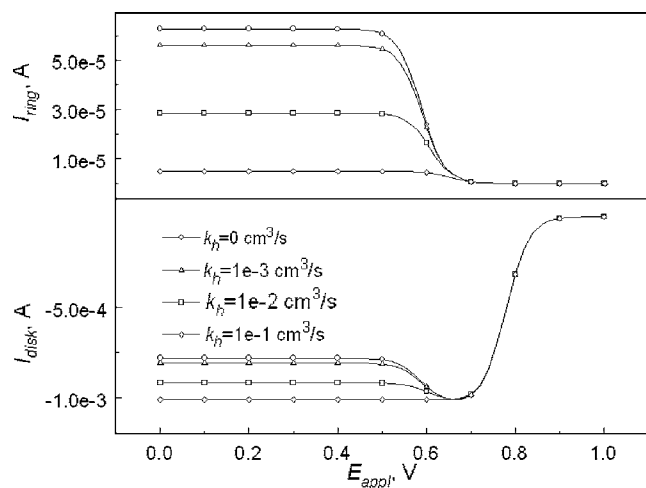


Figure 7. Polarization curves for competing Reactions 1, 2, and 4. Parameters used: $i_{0,1} = 1 \times 10^{-9}$ A/cm², $\alpha_{c,1} = 1.0$, $i_{0,2} = 1 \times 10^{-5}$ A/cm², $\alpha_{c,2} = 1.0$.

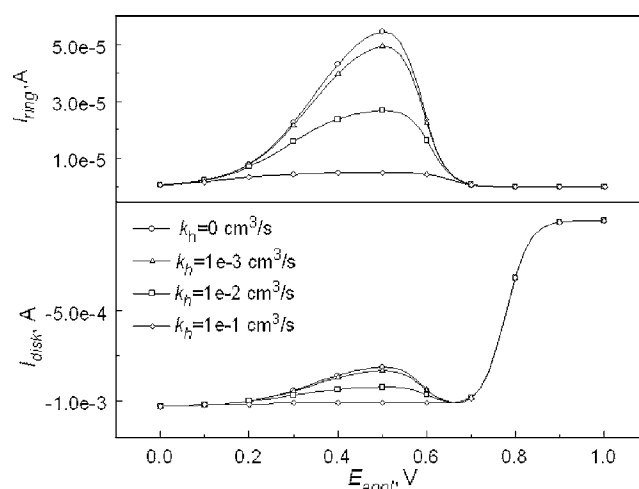


Figure 8. Polarization curves for competing Reactions 1-4. Parameters used: $i_{0,1} = 1 \times 10^{-9}$ A/cm², $\alpha_{c,1} = 1.0$, $i_{0,2} = 1 \times 10^{-5}$ A/cm², $\alpha_{c,2} = 1.0$, $i_{0,3} = 1 \times 10^{-17}$ A/cm², $\alpha_{c,3} = 0.35$.

($c_{\text{H}_2\text{O}_2}$) can be analyzed in a manner similar to that of oxygen, taking into consideration that peroxide is generated on the disk and consumed on the ring.

Potential distribution in the solution phase of the RRDE system is shown in Fig. 10. The parameters used are the same as those used in Fig. 9. The potential is zero at $z = 0.005$ cm, as given by the boundary conditions, and it increases as the distance from the electrode surface decreases. The potential reaches its peak value on the surface of the disk ($r = 0 - 0.3$ cm, $z = 0$) where the ORR occurs. It drops down quickly beyond the disk ($r > 0.3$ cm, $z = 0$), and even quicker adjacent to the surface of the ring ($r = 0.375 - 0.425$ cm) where the anodic reaction occurs. Far away from the disk in the r direction, the liquid potential drops continuously until it reaches the potential of the reference electrode (which is set to 0 V in this work), as shown in Fig. 10. The potential distribution along the z direction is also given in the inserted figure in Fig. 10. Lines for $r = 0.2, 0.34, 0.4$, and 0.6 cm are chosen as they are in the region near the disk, the separator, the ring, and beyond the ring, respectively. The potential is 0 V far away from the electrode surface in the z direction ($z = 0.12$ cm), and it increases as the distance from

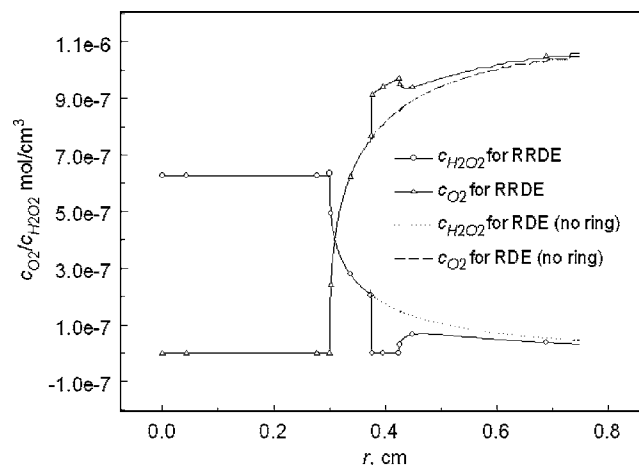


Figure 9. The concentration distribution of O_2 and H_2O_2 along the r direction at the surface of the electrode. Parameters used: $i_{0,1} = 1 \times 10^{-9}$ A/cm², $\alpha_{c,1} = 1.0$, $i_{0,2} = 1 \times 10^{-5}$ A/cm², $\alpha_{c,2} = 1.0$, $i_{0,3} = 1 \times 10^{-17}$ A/cm², $\alpha_{c,3} = 0.35$, $E_{\text{appl}} = 0.5$ V vs SHE.

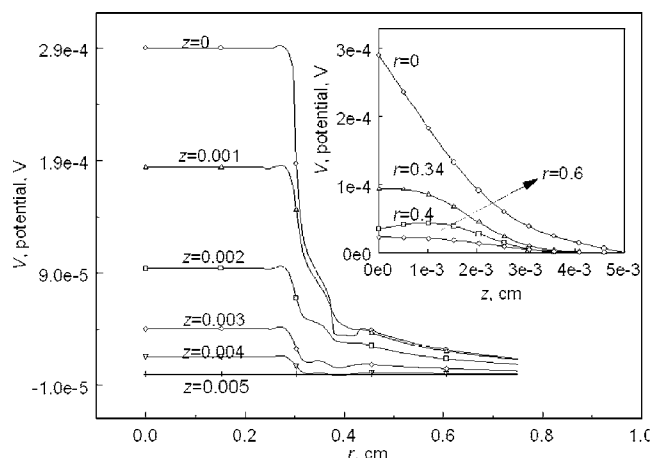


Figure 10. The potential profile along the r and the z direction at the surface of the electrode. Parameters used: $i_{0,1} = 1 \times 10^{-9}$ A/cm², $\alpha_{c1} = 1.0$, $i_{0,2} = 1 \times 10^{-5}$ A/cm², $\alpha_{c2} = 1.0$, $i_{0,3} = 1 \times 10^{-17}$ A/cm², $\alpha_{c3} = 0.35$, $E_{\text{appl}} = 0.5$ V vs SHE.

the electrode surface decreases. The potential increases dramatically near the disk (shown by the line corresponding to $r = 0$) where the cathodic reactions occur. It does not change near the separator and the region beyond the ring (shown by the curves at $r = 0.34$ and 0.6 cm) where no reaction occurs, and it decreases near the ring (as shown by the line corresponding to $r = 0.4$ cm).

Conclusions

The experimentally observed phenomena in polarization curves obtained with RRDE, such as tails and humps, can be explained as the result of the competition between the four-electron transfer reaction and the two-electron transfer reaction, while the peroxide electrochemical reduction and peroxide heterogeneous chemical decomposition reaction can also affect the presence or the size and the position of the humps and the tails. The polarization curves for several combinations of reactions were simulated. The concentration profile of the species involved and potential distribution near the surface of the ring disk electrode were also obtained. Further work is required to attribute the origin of the humps and tails to one mechanism against another.

Acknowledgment

The authors are grateful for financial support provided by the U.S. Department of Energy under cooperative agreement no. DE-FC36-04GO14232.

The University of South Carolina assisted in meeting the publication costs of this article.

List of Symbols

A	area of the disk, cm ²
c_i	concentration of species " i " ($i = 1, 2, 3$, and 4 represent HSO_4^- , H_2O_2 , H^+ , and O_2 , respectively), mol/cm ³
$c_{i,0}$	concentration of species " i " at the surface of the electrode, mol/cm ³
$c_{i,\text{bulk}}$	concentration of species " i " in the bulk solution, mol/cm ³
$c_{i,\text{ref}}$	reference concentration of species " i ", mol/cm ³
$c_{i,\text{RE}}$	concentration of species " i " at the reference electrode, mol/cm ³
D_i	diffusion coefficient of species " i ", cm ² /s
F	Faraday's constant, 96487 C/equiv
$i_{0,\text{ref}}$	exchange current density for reaction " j " at the reference concentrations, A/cm ²
$i_{0,\text{data}}$	exchange current density for reaction " j " at the reference concentrations, A/cm ²
I_L	limiting current calculated using the Levich equation, A
I_R	limiting current collected on the ring, A
I_D	limiting current collected on the disk, A

I_j	current generated by the reaction " j ", A
I_{disk}	current on the disk, A
I_{ring}	current on the ring, A
i_t	total current density defined in Eq. 29, A/cm ²
i_j	current density of the reaction " j ", A/cm ²
k_h	rate constant for the chemical reaction (i.e., Reaction 4) at the electrode surface, mol/s (mol/cm ³)
n_j	stoichiometric number of electrons involved in the electrode reaction " j "
n_{RE}	stoichiometric number of electrons involved in the reaction that occurs at the reference electrode
N	collection efficiency of an RRDE
P	pressure in the electrolyte, Pa
p	reaction order of the non charge transfer reaction (i.e., Reaction 4)
p_{ij}	anodic reaction order of species " i " in reaction " j "
q_{ij}	cathodic reaction order of species " i " in reaction " j "
r	radial distance from the axis of the disk, cm
r_s	rate of chemical reaction (i.e., Reaction 4) at electrode surface, mol/cm ² s
R	gas constant, 8.314 J/mol K
$s_{i,j}$	stoichiometric coefficient of species " i " in the reaction " j "
$s_{i,\text{RE}}$	stoichiometric coefficient of species " i " in the reaction at the reference electrode
T	absolute temperature, K
u_r	radial component of the velocity, cm/s
u_z	axial component of the velocity, cm/s
u_θ	angular component of the velocity, cm/s
$s_{i,\text{RE}}$	stoichiometric coefficient of species " i " in the reaction at reference electrode
U_j^θ	standard electrode potential for the charge transfer reaction " j ", V
$U_{j,\text{ref}}$	open circuit potential of the reaction " j " at the reference concentrations relative to the reference electrode, V
U_{RE}^θ	standard potential of the reference electrode relative to SHE, V
\mathbf{u}	velocity vector, cm/s
z	axial distance, cm
$z_{\infty,v}$	axial distance considered to be sufficiently far from the electrode surface to be considered to be at "infinity" in the domain for the momentum balance, cm
$z_{\infty,m}$	axial distance considered to be sufficiently far from the electrode surface to be considered to be at "infinity" in the domain for material balance, cm
z_i	charge on species " i "

Greek

$\alpha_{a,j}$	anodic transfer coefficient for reaction " j "
$\alpha_{c,j}$	cathodic transfer coefficient for reaction " j "
θ	angular coordinate, rad
ρ	density of the electrolyte, g/cm ³
μ	kinematic viscosity of the electrolyte, mPa s
Φ	potential in solution phase, V
Φ_0	potential in the solution adjacent to the electrode surface, V
Φ_{RE}	potential of the reference electrode at the experimental conditions, V
Φ_{met}	potential of the working electrode, V
Φ_{re}	potential of the reference electrode at the experimental conditions, V
Ω	rotating speed of the electrode, rad/s
η_j	overpotential of reaction " j " corrected for ohmic drop in the solution and measured with respect to a reference electrode of a given kind in a solution at the reference concentrations, V
ΔG_{298}^θ	standard Gibbs free energy change in a chemical process at 298 K, kJ/mol

Subscripts

i	species index, $i = 1, 2, 3$, and 4 represent HSO_4^- , H_2O_2 , H^+ , and O_2 , respectively
j	reaction index, $j = 1, 2, 3, 33, 34$ correspond to Reactions 1, 2, 3, 33, 34, respectively
bulk	properties or variables evaluated at the bulk solution

References

1. E. Endoh, S. Terazono, H. Widjaja, and Y. Takimoto, *Electrochem. Solid-State Lett.*, **7**, A209 (2004).
2. A. B. LaConti, M. Hamdan, and R. C. McDonald, in *Handbook of Fuel Cells, Fundamentals, Technology and Applications*, Vol. 3, W. Vielstich, A. Lamm, and H. A. Gasteiger, Editors, p. 647, Wiley, New York (2003).
3. Q. Guo, P. N. Pintarob, H. Tang, and S. O'Connor, *J. Membr. Sci.*, **154**, 175 (1999).
4. V. Stamenkovic, T. J. Schmidt, P. N. Ross, and N. M. Markovic, *J. Phys. Chem. B*, **106**, 11970 (2002).

5. U. A. Paulus, T. J. Schmidt, H. A. Gasteiger, and R. J. Behm, *J. Electroanal. Chem.*, **495**, 134 (2001).
6. T. J. Schmidt, U. A. Paulus, H. A. Gasteiger, and R. J. Behm, *J. Electroanal. Chem.*, **508**, 41 (2001).
7. V. Srinivasamurthi, R. C. Urian, and S. Mukerjee, in *Proton Conducting Membrane Fuel Cells III*, M. Murthy, T. F. Fuller, J. W. Van Zee, and S. Gottesfeld, Editors, PV 2002-31, p. 99, The Electrochemical Society Proceedings Series, Pennington, NJ (2002).
8. A. J. Bard and L. R. Faulkner, *Electrochemical Methods*, 2nd ed., John Wiley & Sons, New York (2004).
9. M. R. Tarasevich, A. Sadkowsky, and E. Yeager, in *Comprehensive Treatise of Electrochemistry, Kinetics and Mechanisms of Electrode Processes*, Vol. 7, P. Horsman, B. E. Conway, and E. Yeager, Editors, p. 354, Plenum Press, New York (1983).
10. N. M. Markovic, H. A. Gasteiger, and P. N. Ross, Jr., *J. Electrochem. Soc.*, **144**, 1591 (1997).
11. N. M. Markovic, H. A. Gasteiger, and P. N. Ross, Jr., *J. Phys. Chem.*, **99**, 3411 (1995).
12. Y. Mo and D. A. Scherson, *J. Electrochem. Soc.*, **150**, E39 (2003).
13. S. Marcotte, D. Villers, N. Guillet, L. Roue, and J. P. Dodelet, *Electrochim. Acta*, **50**, 179 (2004).
14. B. N. Grgur, N. M. Markovic, and P. N. Ross, *Can. J. Chem.*, **75**, 1465 (1997).
15. U. A. Paulus, A. Wokaun, G. G. Scherer, T. J. Schmidt, V. Stamenkovic, N. M. Markovic, and P. N. Ross, *Electrochim. Acta*, **47**, 3787 (2002).
16. S. L. Gojkovic, S. K. Zecevic, and R. F. Savinell, *J. Electrochem. Soc.*, **145**, 3713 (1998).
17. V. S. Murthi, R. C. Urian, and S. Mukerjee, *J. Phys. Chem. B*, **108**, 11011 (2004).
18. E. Claude, T. Addou, J. M. Latour, and P. Aldebert, *J. Appl. Electrochem.*, **28**, 57 (1998).
19. S. Chen and A. Kucernak, *J. Phys. Chem. B*, **108**, 3262 (2004).
20. F. M. White, *Viscous Fluid Flow*, McGraw-Hill, Inc., New York (1974).
21. J. Newman and K. E. Thomas-Alyea, *Electrochemical Systems*, 3rd ed., John Wiley & Sons, Hoboken, NJ (2004).
22. R. E. White, C. M. Mohr, Jr., and J. Newman, *J. Electrochem. Soc.*, **123**, 383 (1976).
23. J. F. Yan, T. V. Nguyen, R. E. White, and R. B. Griffin, *J. Electrochem. Soc.*, **140**, 733 (1993).
24. P. K. Adanuvor and R. E. White, *J. Electrochem. Soc.*, **134**, 1093 (1987).
25. R. E. White and S. E. Lorimer, *J. Electrochem. Soc.*, **130**, 1096 (1983).
26. R. E. White, S. E. Lorimer, and R. Darby, *J. Electrochem. Soc.*, **130**, 1123 (1983).
27. P. K. Adanuvor, R. E. White, and S. E. Lorimer, *J. Electrochem. Soc.*, **134**, 625 (1987).
28. R. B. Bird, W. E. Stewart, and E. N. Lightfoot, *Transport Phenomena*, 2nd ed., John Wiley & Sons, New York (2002).
29. W. J. Albery and S. Bruckenstein, *Trans. Faraday Soc.*, **62**, 1920 (1966).
30. W. H. Smyrl and J. Newman, *J. Electrochem. Soc.*, **119**, 212 (1972).
31. C. F. Zinola, A. M. C. Luna, W. E. Triaca, and A. J. Arvia, *Electrochim. Acta*, **39**, 1627 (1994).
32. O. Antoine and R. Durand, *J. Appl. Electrochem.*, **30**, 839 (2000).
33. M. F. Easton, A. G. Mitchell, and W. F. K. Wynne-Jones, *Trans. Faraday Soc.*, **48**, 796 (1952).